Nucleolar stress causes the entry into replicative senescence in budding yeast

Sandrine Morlot[1234*], Song Jia[1234], Isabelle Léger-Silvestre[5], Audrey Matifas[1234], Olivier Gadal[5], Gilles Charvin[1234*].

[1]Developmental Biology and Stem Cells Department, Institut de Génétique et de Biologie Moléculaire et Cellulaire, Strasbourg, France;

[2]Centre National de la Recherche Scientifique, Illkirch, France;

[3]Institut National de la Santé et de la Recherche Médicale, Illkirch, France;

[4]Université de Strasbourg, Illkirch, France;

[5]Laboratoire de Biologie Moléculaire Eucaryote, Centre de Biologie Intégrative (CBI), Université de Toulouse, CNRS, UPS, Toulouse 31000, France;

*Correspondence: morlot@igbmc.fr charvin@igbmc.fr

Key words: Live cell imaging, microfluidics, ribosome biogenesis, replicative aging

Summary

The accumulation of Extrachromosomal rDNA Circles (ERCs) and their asymmetric segregation upon division have been hypothesized to be responsible for replicative senescence in mother yeasts and rejuvenation in daughter cells. However, it remains unclear by which molecular mechanisms ERCs would trigger the irreversible cell cycle slow-down leading to cell death. We show that ERCs accumulation is concomitant with a nucleolar stress, characterized by a massive accumulation of pre-rRNAs in the nucleolus, leading to a loss of nucleus-to-cytoplasm ratio, decreased growth rate and cell-cycle slow-down. This nucleolar stress, observed in old mothers, is not inherited by rejuvenated daughters. Unlike WT, in the long-lived mutant *fob1Δ,* a majority of cells is devoid of nucleolar stress and does not experience replicative senescence before death. Our study provides a unique framework to order the successive steps that govern the transition to replicative senescence and highlights the causal role of nucleolar stress in cellular aging.

Introduction

Budding yeast cells undergo a limited number of asymmetrical divisions before entering senescence and eventually dying, a phenomenon known as replicative aging (Mortimer and Johnston, 1959). Unlike symmetrically dividing unicellular organisms (Nakaoka and Wakamoto, 2017; Spivey et al., 2017), the replicative lifespan (RLS) in budding yeast follows a broad Gaussian distribution within a population, indicating that cell death is not a stochastic

process, yet presents large cell-to-cell variability. Importantly, while the replicative age of mothers increases at each division, new born daughter cells recover a full replicative potential (Kennedy et al., 1994). Such rejuvenation of daughter cells led to postulate that cell death results from the accumulation of aging factors in mothers, which are asymmetrically segregated upon cell division (Egilmez and Jazwinski, 1989).

The accumulation of Extrachromosomal ribosomal DNA Circles (ERCs) in aging mothers was the first potential aging factor that was studied in detail (Sinclair and Guarente, 1997). ERCs result from the excision of repeats from the rDNA cluster located on chromosome XII. This genomic region contains the highly transcribed 35S ribosomal RNA genes in tandem repeats (approximately 150 copies). A replication fork barrier (RFB), where the protein Fob1 binds, prevents the collision between the replication fork and the RNA polymerase I transcription of 35S rRNA gene (Brewer and Fangman, 1988; Kobayashi, 2003). The repetitive nature of the rDNA cluster and the stalling of the DNA replication complex at the RFB, which favors double strand breaks, promote recombination events. ERCs were shown to progressively accumulate in aging cells due to the presence of an autonomously replicating sequence (ARS) on each rDNA repeat, that ensures the amplification of the excised DNA circles over successive divisions (Sinclair and Guarente, 1997). Strains deleted for the *FOB1* gene present lower amount of ERCs and an extended lifespan (Defossez et al., 1999) which further correlates accumulation of ERCs with replicative aging. Finally, to explain daughter rejuvenation with the ERC accumulation model, it was proposed that a diffusion barrier at the bud neck prevents the ERCs from being inherited by the daughter cells during cell division (Denoth-Lippuner et al., 2014; Shcheprova et al., 2008).

However, maintaining low ERC levels by genetically decreasing the recombination probability at the rDNA locus is not enough to promote longevity (Ganley et al., 2009). Furthermore, it is not clear why ERC accumulation is toxic to the cell and how it would lead to an arrest of proliferation (Ganley and Kobayashi, 2014). Another hypothesis favors rDNA instability, in particular the activity of the non-coding bidirectional promoter, called Epro, which is responsible for the amplification of rDNA repeats, rather than ERCs accumulation as being involved in replicative aging (Kobayashi, 2008; Saka et al., 2013). Hence, the mechanism that links rDNA regulation and replicative aging remains to be elucidated.

62 The dynamics of aging in budding yeast has been previously characterized by an abrupt
63 transition, called the Senescence Entry Point (SEP), between an healthy state with regular and
64 robust divisions and a senescent-like state where cell cycles are much longer and variable
65 (Fehrmann et al., 2013). The molecular pathways responsible for this abrupt cellular transition
66 are still not understood. In particular, it is not known how ERCs, rDNA instability and nucleolar
67 activity, good candidates for aging factors, are linked to the SEP.

68 In this study, we analyzed in vivo the aging process in single yeast cells over multiple
69 generations using microfluidic tools and time lapse microscopy. We show that a dramatic
70 nucleolar stress combined with the accumulation of ERCs precede the SEP. This nucleolar
71 stress is characterized by an upregulation of rDNA transcription and an accumulation of pre-
72 rRNAs in the nucleolus followed, by an enlargement of the nucleus concomitantly with the
73 irreversible cell cycle slow-down. Altogether, these findings highlight that the nucleolar steps
74 of ribosome biogenesis play a critical role in the entry of replicative senescence.

75 **Results**

76 **The number of rDNA repeats and the nucleolar volume increase before the irreversible cell**
77 **cycle slow-down leading to cell death**

78 To follow the real-time dynamics of the rDNA cluster during replicative aging in individual
79 yeast cells, we used a previously developed strain (Miyazaki and Kobayashi, 2011), in which
80 LacO sequences are inserted in all repeats of the rDNA array (Fig1A and Movie S1). In this
81 strain, the protein Net1, involved in nucleolar silencing, telophase exit and stimulation of RNA
82 Pol I-mediated transcription, is labelled with mCherry, which allows detecting the nucleolus.
83 Thus, by monitoring GFP-LacI signal within the nucleolus delimited by NET1-mCherry
84 fluorescence, we could estimate the evolution of rDNA repeats number in single mother cells
85 trapped from birth to death in a microfluidic device (Fig1A), as previously described (Goulev
86 et al., 2017). The senescence entry point (SEP) is a particularly critical time point in yeast
87 lifespan as it corresponds to the abrupt cell cycle slow-down occurring before cell death (Fig1B
88 and 1C) (Fehrmann et al., 2013). We thus analyzed fluorescence signals after SEP alignment
89 rather than birth alignment which blurs the cell cycle dynamics and does not allow to order
90 cellular events (FigS1A). We observed that the total GFP-LacI fluorescence within the
91 nucleolus increased significantly by 60% within the 5 divisions preceding SEP and further
92 increased to 4.4-fold 5 divisions after SEP (Fig1D). If considering 150 repeats as the basal size

93 of the rDNA cluster, fluorescence measurements allow us to estimate an increase to 240
94 repeats before SEP and to more than 600 repeats after SEP. This increase is likely to originate
95 from ERCs accumulation as wild type cells hardly accumulate more than 200 repeats within
96 the rDNA cluster (Ide et al., 2013). In agreement with this result, we also found an increased
97 signal of FOB1-GFP before SEP (FigS1B), which suggests a higher rate of blocked replication
98 forks at RFB before SEP and thus a higher rate of ERCs production.

99 Interestingly, NET1-mcherry signal increased to a larger extent than GFP-LacI before (3.9-fold)
100 and after SEP (25-fold) (Fig1E and FigS1E). The nucleolar size has been shown to correlate
101 positively with the cellular volume (Jorgensen et al., 2007). However, the sudden increase in
102 NET1-mCherry signal was not due to an abrupt cell size enlargement as the cell area dynamics
103 did not vary much during the SEP transition (FigS1C). This increase of NET1-mCherry
104 fluorescence was mainly due to an enlargement of the nucleolar volume as NET1-mCherry
105 mean fluorescence increases only by 36% after SEP (FigS1E) which was much lower than the
106 17-fold increase of the segmented area (FigS1D).

107 These results highlight that the nucleolus undergoes two major modifications prior to entry
108 into cellular senescence: an increased copy number of ribosomal RNA genes and a volume
109 expansion.

110 **A massive upregulation of rDNA transcription and of pre-rRNAs processing precedes the**
111 **entry into senescence**

112 We found a dramatic increase in the nucleolar volume occurring before the SEP. The nucleolus
113 is the nuclear region were pre-rRNAs are synthetized and processed. Therefore, we
114 investigated how rDNA transcription and pre-rRNAs levels evolve during the SEP transition.

115 To this end, we first monitored the total amount of RNA Pol1 by following its largest subunit
116 RPA190, fused to GFP, throughout yeast lifespan (Fig2A and Movie S2). We measured an
117 increase by 70% in RPA190-GFP total fluorescence over the 5 divisions preceding SEP, followed
118 by a larger increase (up to 7-fold) after SEP (Fig2B). Next, to establish if this increased level of
119 RNA Pol1 led to higher transcription at the rDNA locus, we measured the amount of pre-rRNAs
120 in the nucleolus by performing RNA FISH on aging cells directly in the microfluidic chip
121 (referred to as “FiSH on Chip” in the following). For this, we stopped the time-lapse experiment
122 after 60 hours acquisition, when the microfluidic device was fully loaded and the ages of

123 trapped mother cells were spread before and after SEP, as cells growing in cavities were not
124 synchronized (left graphs Fig2C and 2D). We then performed RNA FISH staining on chip after
125 cell fixation and cell wall digestion. The FISH probe targeted specifically the ITS1 region so that
126 all pre-rRNAs from 35S to 20S would be labelled. FISH staining and RPA190-GFP signal
127 presented a good colocalization, as expected (panels in Fig2C and 2D). For cells in a pre-SEP
128 state (constant and short division timings), we measured a strong positive correlation (black
129 dots in Fig2C, Pearson corr. coef. = 0.8) between the fluorescence levels of FISH probes and
130 RPA190-GFP, indicating that the amount of pre-rRNAs scaled with the amount of RNA Pol1.
131 For cells having already experienced SEP before fixation and FISH staining, the positive
132 correlation remained, even though to a lower extent (magenta stars in Fig2C, Pearson corr.
133 coef. = 0.5) (Fig2C), suggesting that the amount of RNA Pol1 and the rate of transcription could
134 be uncoupled after entry into senescence. We measured a 4.4-fold increased amount of RNA
135 Pol1 and a 2.6-fold increase of pre-rRNAs after the SEP transition (boxplot Fig2C). These results
136 show that pre-rRNAs undergo a massive nucleolar accumulation upon the SEP.

137 As RNA Pol1 showed an increasing amount before SEP (Fig. 2A), we tested whether pre-rRNAs
138 levels followed a similar trend. To address this question, we focused on pre-SEP cells (black
139 dots on Figure 2C) and compared 'early pre-SEP' cells (blue diamonds in Fig2D) having
140 experienced less than 5 divisions with 'late pre-SEP' cells (green dots in Fig 2D) having
141 undergone more than 10 divisions. 'Late pre-SEP' cells are more likely than 'early pre-SEP' cells
142 to be close to the SEP and thus to present a higher level of RPA190-GFP. Indeed, we measured
143 a 3.8-fold increase of RPA190-GFP fluorescence in the 'late pre-SEP' cells (boxplot Fig2D). We
144 observed a good correlation between RNA Pol1 amount and FISH fluorescence in the 2
145 subgroups (Pearson corr. coeff. = 0.8 for 'early pre-SEP' and 0.7 for 'late pre-SEP', Figure 2D).
146 Moreover, we measured a 3.9-fold increase in the pre-rRNAs levels in the 'late pre-SEP' cells,
147 similar to the 3.8-fold increase in Pol1 levels (Fig2D). These results show that pre-rRNAs levels
148 follow a dynamics very similar to RNA Pol1 before SEP. We thus conclude that the onset of
149 accumulation of pre-rRNAs in the nucleolus precedes the entry into replicative senescence.

150 As the RNA FISH experiment could not discriminate between the successive transient pre-
151 rRNAs from 35S to 20S, we could not determine whether rRNA processing was upregulated
152 before SEP. Since SSF1 is a component of the 66S pre-ribosomal particles, we hypothesized
153 that the level of this protein should follow the increase in pre-rRNA levels if rRNA processing

154 was upregulated accordingly upon the SEP. Therefore, we monitored SSF1 protein fused to
155 GFP throughout aging (Fig2E and Movie S3). Similarly to pre-rRNA levels, we observed that
156 SSF1-GFP fluorescence increased by 4.2-fold before and up to 24-fold after SEP (Fig2E). These
157 results show that both co- and post-transcriptional processing of pre-rRNAs are upregulated
158 during the 5 divisions before SEP. These results suggest that the entry into senescence is
159 preceded by a massive increase in the demand of ribosomal biogenesis that goes well beyond
160 physiological growth requirements and results in the accumulation of pre-rRNAs in the
161 nucleolus.

162 **The up-regulation of pre-rRNAs synthesis does not lead neither to an increase in ribosomes**
163 **levels nor to a higher growth rate**

164 Since senescent cells undergo a large accumulation of pre-ribosomes, we wondered whether
165 this process was ultimately accompanied by a larger production of ribosomes and, eventually,
166 an increase of the growth rate. First, we sought to evaluate if the nuclear export of pre-RNAs
167 was following the same dynamics as the earlier steps of ribosome biogenesis.

168 To this end, we reasoned that the export rate of pre-rRNAs should scale with the amount of
169 NOG2, which is a protein required for late pre60S ribosome maturation in the nucleoplasm
170 and nuclear export. By monitoring the fusion NOG2-GFP (Fig3A and Movie S4), we measured
171 a good scaling of fluorescence levels with the cell area before SEP (Fig3B and FigS2A), in sharp
172 contrast with the levels of RPA190-GFP and SSF1-GFP, which increased much faster than cell
173 area from 5 divisions before SEP (Fig3G, 3H, S2D and S2E). Hence, our results suggest that the
174 constant basal rate of nucleoplasmic maturation of pre-ribosomes is uncoupled to the
175 upregulation of the nucleolar steps of ribosome biogenesis.

176 Next, we investigated whether the cytoplasmic level of ribosomes was modified during the
177 SEP transition by following RPL13A, a component of the 60S ribosomal subunit, fused to GFP
178 (Fig3C and Movie S5)(Janssens and Veenhoff, 2016). Similarly to NOG2-GFP, we observed a
179 constant ratio of RPL13A-GFP over the cellular area before SEP (Fig3D and FigS2B), indicating
180 that the cytoplasmic concentration of ribosomes remained constant during the SEP transition,
181 in striking contrast with the massive upregulation of early steps of ribosome biogenesis in the
182 nucleolus.

183 Finally, we estimated the growth rate based on the segmented contours in phase contrast of
184 mother and daughter cells (Fig3E). In healthy cells, the activation of ribosome biogenesis in
185 the nucleolus normally responds to a higher demand in growth. In contrast, in aging cells
186 experiencing a nucleolar expansion, we observed a constant growth rate until the SEP (Fig3F
187 and FigS3C) in agreement with the constant concentration of ribosomes. Strikingly the growth
188 rate started to significantly decrease at the SEP (Fig3F and FigS2C), while this dynamics is not
189 noticeable for RPL13A-GFP and NOG2-GFP where a slight decrease occurred only several
190 divisions after SEP (Fig3B and 3D). These results suggest that senescent cells undergo a
191 nucleolar stress where nucleolar ribosome biogenesis, cytosolic ribosome levels and growth
192 rate are uncoupled.

193 **The SEP is concomitant with a large increase in nucleoplasmic content.**

194 As the nucleolar volume drastically increased before SEP compared to the cell volume (Fig3I),
195 we looked at the dynamics of the whole nucleus. We measured the nucleus size with the
196 nuclear reporter HTB2-sfGFP (Fig3J and Movie S6). We observed an abrupt increase in nuclear
197 content, concomitantly with the SEP (Fig4D). This increase resulted in a striking loss of the
198 nuclear to cellular volume ratio or N/C ratio (Fig3K and 4E). Importantly, this behavior is not
199 specific to histones, as we observed the same dynamics with the nuclear reporter NLS-sfGFP
200 under the control of *ACT1* promoter (FigS2F). Using the NLS-sfGFP reporter, the increase in
201 N/C ratio occurred slightly before the SEP. We explain this difference by the fact that, with the
202 NLS-sfGFP reporter, we followed the whole nucleus including the nucleolus, whereas with
203 HTB2-sfGFP, we mainly measured the nucleoplasmic volume, as the nucleolus contains a low
204 level of histones. Removing the NLS sequence abolished the sudden increase in sfGFP
205 fluorescence at SEP (FigS2G), further highlighting the specific dynamics of the nucleus. The
206 increase in N/C ratio is also peculiar when compared to the other organelles such as the
207 vacuoles. Indeed using the vacuolar marker VPH1-GFP, we measured that the vacuole
208 occupies a constant fraction of 30% of the cellular area throughout lifespan (FigS2H), while
209 the nuclear area represents 10% of the cellular area before SEP and suddenly increases up to
210 40% after SEP (Fig3K, S2F, 4E). In addition, high N/C ratio is an unexpected feature of aging
211 cells as this ratio is known to be strongly robust in wild type young yeast cells and in numerous
212 mutants including cell size and cell cycle mutants (Jorgensen et al., 2007; Neumann and Nurse,

213 2007). Therefore the loss of N/C ratio, as a non-physiological characteristics, could be
214 mechanistically linked to the irreversible cell cycle slow-down leading to cell death.

215 **Nucleolar stress is not transmitted to rejuvenated daughter cells**

216 We have identified a nucleolar stress occurring in aging mother cells characterized by an
217 upregulation, in the nucleolar steps, of ribosome biogenesis which is inefficient in producing
218 more ribosomes and in increasing growth (Fig3L). This event was found to be tightly related
219 to – and even preceded- the cell cycle slow-down that defines the SEP. According to the yeast
220 replicative aging paradigm, daughters of aging mothers recover a full replicative potential, as
221 putative aging markers are not transmitted to daughter cells (Kennedy et al., 1994). In the
222 following, we sought to investigate whether our model of entry into senescence triggered by
223 a nucleolar stress was compatible with the previously reported daughter rejuvenation.

224 To this end, first, as a proxy for assessing the recovery of physiological function in new born
225 daughters, we measured the division time of daughters of aging mothers. For this, we took
226 advantage of the cavities in our microfluidic device which allowed tracking of the daughter
227 lineage of trapped mother cells for a couple of divisions. Strikingly, we found that the daughter
228 cells of post-SEP mothers recovered a cell cycle duration that was identical to pre-SEP cells
229 (Fig4A). This revealed that one single division was sufficient to remove the deleterious effects
230 of replicative aging on cell cycle progression.

231 Then, we asked whether this rejuvenation process was driven by an asymmetrical segregation
232 of the nucleolar stress markers upon division. Specifically, as RNA Pol1 and pre-rRNAs were
233 both shown to increase in mother cells prior to SEP, we measured the fluorescence of RPA190-
234 GFP and SSF1-GFP markers in the successive daughters of aging mother cells. Remarkably,
235 daughter cells were born with a constant basal amount of these proteins even when the levels
236 increased in mothers after the SEP (Fig4B and 4C). This demonstrated that daughter cells
237 recovered basal levels of rDNA transcription and pre-rRNAs processing even when the mother
238 acquired a strong senescence-associated impairment in nucleolar activity.

239 To further investigate the mechanism at stake in the segregation of age between mothers and
240 daughters, we measured the nuclear size in daughters of aging mothers based on HTB2-sfGFP
241 fluorescence. Importantly, we observed that daughters of post-SEP mothers inherited a
242 nucleus of basal size despite the large increase in nuclear size in their mothers (Fig4D).

243 Similarly, the N/C ratio was also rescued in daughter cells (Fig4E), further illustrating that
244 daughters had recovered a normal physiology (Fig4F). Altogether, these results revealed the
245 existence of an efficient rejuvenation mechanism based on asymmetrical partitioning of the
246 nucleus/nucleolus upon division, which prevents the inheritance of nucleolar stress in new
247 born daughters.

248 **Fob1 ties the onset of nucleolar stress to the entry into senescence**

249 The fact that a nucleolar stress consistently occurs ahead of the onset of cell cycle slow-down
250 upon entry into senescence argues in favor of a mechanistic link between these two events.
251 To further establish their causality, we used the *fob1* mutant to perturb the stability of the
252 rDNA and assess its consequence on the dynamics of entry into senescence.

253 The mutant fob1Δ has been shown to present a lifespan extension of 30% compared to wild
254 type (Defossez et al., 1999). Measurements in our microfluidic device confirmed the enhanced
255 longevity of this mutant (Table 1, Fig5A). Interestingly, a large majority (68.3%) of *fob1*Δ cells
256 does not present any cell cycle slow-down before death while only 7% of WT cells have no SEP
257 transition (Table1, Fig5B and 5C). These *fob1*Δ cells without SEP (referred to as 'fob1Δ NO SEP'
258 in the following) present a further increased lifespan (RLS=37, Fig5A) than the fob1Δ cells
259 experiencing a SEP (referred to as '*fob1*Δ with SEP', RLS=34, still longer-lived than WT).
260 Interestingly, in '*fob1*Δ with SEP', the onset of cell cycle slow-down is delayed (Table1) but the
261 dynamics of the cell cycle slow-down is similar to WT (Fig5D). It is worth noticing that WT,
262 'fob1Δ with SEP' and 'fob1Δ NO SEP' populations have similar cell area dynamics (FigS3A)
263 when aligned from birth. When aligned from SEP, fob1Δ cells present a slightly larger area at
264 SEP than WT cells (FigS3B) showing that SEP is not triggered by a cellular volume threshold.
265 These results suggest that the observed differences with respect to the entry into senescence
266 cannot be attributed to cell size effects and reinforce the idea that cell size is not an aging
267 factor.

268 Altogether, these results indicate that a common mechanism may be at stake in the
269 progression through senescence *(i.e.* in the post-SEP period of the lifespan) in both WT and
270 *fob1*Δ mutant. However, it suggests that the SEP trigger is a stochastic event, the probability
271 of which is determined by Fob1, presumably through the control of the rDNA instability.

272 To further check this hypothesis, we analyzed the fluorescence of RPA190-GFP, subunit of RNA
273 Pol1 in the two *fob1*Δ subpopulations. The population '*fob1*Δ with SEP' experienced a
274 significant increase of RPA190-GFP fluorescence before SEP similar to WT and cells died with
275 a large amount of RNA Pol1 (Fig5F and Movie S8). In contrast, the '*fob1*Δ NO SEP' population
276 kept a basal level of RPA190-GFP throughout lifespan (Fig5G) and cells died with a
277 physiological level of RNA Pol1 even after more than 30 divisions (Fig5E and Movie S7).
278 Daughter cells of both populations '*fob1*Δ NO SEP' and '*fob1*Δ with SEP' recover similar levels
279 of RPA190-GFP (FigS3C), showing that the maintenance of small nucleoli in '*fob1*Δ NO SEP' is
280 not due to an impaired asymmetrical nuclear segregation upon division but rather to a better
281 homeostasis of nucleolar activity during aging.

282 Similarly, we measured the fluorescence of the nuclear marker HTB2-sfGFP in the two
283 populations 'fob1Δ NO SEP' and 'fob1Δ with SEP'. In agreement with the nucleolar markers,
284 only the cells experiencing a SEP presented an increased level of HTB2-sfGFP very similar to
285 WT (Fig5H). We also calculated the growth rate of *fob1*Δ cells. In agreement with the 2
286 previous senescence markers (cell cycle slow-down and increased nuclear size), '*fob1*Δ with
287 SEP' population presented a decreased growth rate at SEP similar to WT while '*fob1*Δ NO SEP'
288 cells maintained a constant growth rate throughout lifespan (FigS3D).

289 In conclusion, we show that the FOB1-dependent onset of nucleolar stress predicts, in the
290 following 5 divisions, the entry into replicative senescence, characterized by sudden cell cycle
291 slow down, decreased growth rate and nuclear enlargement.

292 **Discussion**

293 By combining microfluidics, time-lapse microscopy and quantitative single cell analysis, we
294 have uncovered that nucleolar stress is a predictive marker of imminent entry into
295 senescence. Alignment from SEP was a key methodological breakthrough to chronologically
296 order the molecular events leading to cell death. Indeed, when data were aligned from cell
297 birth, as it is usually performed, all parameters gave similar gradual dynamics, which does not
298 allow to distinguish causes from consequences (FigS1A). By aligning single cell trajectories
299 from SEP, we identified that the nucleolar initiation of ribosome biogenesis is upregulated in
300 a FOB1-dependent-way and is followed, within 5 divisions, by a massive nuclear enlargement,
301 a decreased growth rate and the irreversible cell cycle slow-down, leading eventually to cell
302 death (Fig3L and 4F). Thus, our results contradicts the classical paradigm of a progressive

303 decline in physiological functions during aging and highlights the nucleolar stress as a critical
304 step during replicative aging.

305 Ribosome biogenesis has been previously identified as a key pathway involved in yeast
306 replicative aging. Indeed, in a genome-wide analysis of aged-sorted cell populations
307 combining both mRNA sequencing and mass spectrometry, the authors showed that the
308 transcription of protein biogenesis-related genes gets uncoupled, with age, from the
309 translation of corresponding mRNAs (Janssens et al., 2015). They further suggested, based on
310 computational analysis, that this uncoupling could likely cause replicative aging. In agreement
311 with this study, we described a detailed molecular mechanism connecting the dysregulation
312 of ribosome biogenesis, characterized by the uncoupling between pre-rRNAs synthesis and
313 ribosomes maturation, to cellular aging. We established that a stochastic event triggers this
314 nucleolar stress (and subsequently cellular senescence) almost systematically in WT cells and
315 in a small fraction of *fob1*Δ cells. ERCs excision and/or rDNA cluster amplification are very
316 likely to be this stochastic event as FOB1 regulates these processes (Defossez et al., 1999;
317 Kobayashi et al., 1998). In wild type cells, ERCs are generated by the FOB1-dependent stalling
318 of the replication fork at RFB, whereas in *fob1*Δ cells, ERCs are produced by the collision of the
319 replication fork against RNA Pol1 transcription machinery (Takeuchi et al., 2003). This latter
320 event occurs less frequently than FOB1-dependent excision as only half of 35S genes are
321 actively transcribed (Dammann et al., 1993) and less than one third of ARS, in the rDNA cluster,
322 are fired during S phase (Brewer and Fangman, 1988). Thus, some *fob1*Δ cells would never
323 experience any ERC excision event during their lifespan. This would explain the two sub-
324 populations "*fob1*Δ NO SEP" and "*fob1*Δ with SEP" that we identified. Our results also
325 identified an atypical activation of rDNA transcription leading to cellular senescence. Indeed
326 we show that the increased number of ribosomal RNA genes and the enhanced activity of RNA
327 Pol1 are a unique feature of aging cells close to the senescence transition; as in healthy young
328 yeast cells, RNA Pol1 activity is up-regulated, in a compensatory mechanism, only when the
329 number of repeats in the rDNA cluster is reduced (Takeuchi et al., 2003).

330 We meticulously characterized the entry into senescence as the simultaneous onset of three
331 sudden major cellular alterations: cell cycle slow down, decreased growth rate and nuclear
332 enlargement. It still remains to be determined the precise interplay between these three
333 physiological modifications and how they lead to cell death. The massive nuclear enlargement

334 and the subsequent loss of N/C ratio at SEP are striking aging markers as the nuclear volume
335 should normally robustly scale with the cellular volume (Neumann and Nurse, 2007). It has
336 recently been shown that disrupting mRNA export machinery in *S. pombe* increases
337 significantly the N/C ratio by accumulation of RNAs (Kume et al., 2017). In addition, premature
338 rRNAs are known to be trapped within the nucleolus (Gadal et al., 2002). The transition from
339 the nucleolus to the nucleoplasm is accompanied by major compositional changes in
340 preribosome (Kressler et al., 2017). Thus, the dramatic accumulation of pre-rRNAs, trapped in
341 the nucleolus, could probably result in the accumulation of further nuclear intermediates
342 involved in ribosome biogenesis and be directly responsible for the sudden loss of N/C ratio
343 during replicative aging. This abrupt increase in nuclear volume, together with the
344 accumulation of nuclear proteins, might then trigger a pathway slowing down cell cycle to
345 allow the cell to reach a volume matching its nuclear size. However, pre-ribosomal particles
346 synthetized in senescent cells are not export-competent and remain in the nucleolus.
347 Therefore, growth rate does not increase, thus cellular volume never catches up the
348 appropriate physiological N/C ratio, reinforcing the activation of the pathway slowing down
349 cell cycle, which could explain the irreversibility of the senescent state.

350 The nucleolar mechanism described in this study is likely conserved across species as similar
351 observations were also reported in several studies in metazoans. In the germline stem cells of
352 Drosophila male, the rDNA array on chromosome X is silenced in young flies but active in old
353 flies (Lu et al., 2018). In mouse embryonic fibroblasts, oncogenic stress induces rRNA
354 transcription and triggers cellular senescence (Nishimura et al., 2015). Our data precise that
355 the transcription at the rDNA cluster is activated before the onset of cellular senescence in
356 physiological conditions (no external induction of senescence). In particular, our work clearly
357 demonstrates that nucleolar dysregulation is not a mere consequence of the aging process
358 but appears before the establishment of a senescent state. More recently, it has been found
359 that small nucleoli in post-mitotic cells are a hallmark of an extended longevity in *C. elegans*,
360 Drosophila, Mice and human muscle tissues (Tiku et al., 2016). These results, together with
361 our study, highlight the crucial role of the nucleolus in both replicative and chronological
362 aging, suggesting the existence of a global and conserved nucleolar mechanism controlling
363 longevity.

364

365 **Figure legends**

366 **Figure 1: The number of rDNA repeats and the nucleolus size increase 5 divisions prior to**
367 **SEP.** (A) Top: sketch of LacO insertion on each rDNA repeat in a strain containing NET1-
368 mCherry and GFP-LacI. Bottom: pictures of a mother cell, delimited by a yellow contour in the
369 fluorescence channels, with GFP-LacI and NET1-mCherry markers, trapped in a cavity in a
370 microfluidic device from birth to death. Scale bar: 5µm. (B) Left: duration of successive cell
371 cycles for 3 single cells (magenta, cyan and orange). Middle: Average cell cycle duration as a
372 function of age for single cell trajectories aligned from birth. (C) Left: same 3 single cells as in
373 B aligned from SEP. Middle: Average cell cycle durations after SEP alignment. Right:
374 normalized cell cycle duration for 4 classes of age: (1): more than 5 divisions before SEP, (2):
375 5 to 0 divisions before SEP, (3): 1 to 5 divisions after SEP and (4): more than 5 divisions after
376 SEP; data are normalized to the average of the 1st class. (D) Total GFP-LacI fluorescence
377 (arbitrary units) within the contour delimited by NET1-mCherry signal for the same 3 single
378 cells as above (left) and averaged after SEP alignment (middle). Right: normalized GFP-LacI
379 fluorescence for 4 classes of age. (E) Total NET1-mCherry fluorescence (arbitrary units) for the
380 same 3 single cells as above (left) and averaged after SEP alignment (middle). Right:
381 normalized NET1-mCherry fluorescence for 4 classes of age. N=49 mother cells (for all
382 averaged curves).

383 **Figure 2: rRNAs synthesis and processing are upregulated before SEP.** (A) Mother cell with
384 RPA190-GFP marker in a microfluidic chip. (B) Total RPA190-GFP fluorescence (arbitrary units)
385 for 3 single cells (left) and averaged after SEP alignment (middle). Right: normalized RPA190-
386 GFP fluorescence for 4 classes of age. N=61 cells. (C) and (D) FISH on CHIP. Left: examples of
387 cell cycle trajectories and corresponding pictures of cells labeled by RNA FISH directly on the
388 microfluidic chip after 60 hours time-lapse acquisition. Middle: RPA190-GFP fluorescence as a
389 function of FISH probe fluorescence. Right: boxplot of relative fluorescence of RPA-190 and
390 FISH probe for pre-SEP cells (N= 136 cells, black in C), post-SEP cells (N= 123 cells, magenta in
391 C), early pre-SEP cells (N= 45 cells, blue in D) and late pre-SEP cells (N= 68 cells, green in D).
392 (E) Left: mother cell with SSF1-GFP marker in a microfluidic chip. Middle: total SSF1-GFP
393 fluorescence averaged after SEP alignment. Right: normalized SSF1-GFP fluorescence for 4
394 classes of age. N= 56 cells. Scale bar: 5µm (for all pictures).

395 **Figure 3: Ribosome concentration and growth rate do not increase during the entry into**
396 **senescence.** (A) Mother cell with NOG2-GFP marker on a microfluidic chip before and after
397 SEP. (B) Ratio of NOG2-GFP total fluorescence over cellular area as a function of generation,
398 averaged after SEP alignment. N= 33 cells. (C) Mother cell with RPL13A-GFP marker on a
399 microfluidic chip before and after SEP. (D) Ratio of RPL13A-GFP total fluorescence over cellular
400 area as a function of generation, averaged after SEP alignment. N= 32 cells. (E) Sketch
401 explaining the calculation of growth rate based on segmented contour of the mother cells
402 before budding (light green), the mother cell at the end of the division (dark green) and the
403 new born daughter (orange). (F) Growth rate (measured from projected area) as a function of
404 generation, averaged after SEP alignment. N=36 cells. (G) Ratio of RPA190-GFP total
405 fluorescence over cellular area as a function of generation averaged after SEP alignment. N=
406 61 cells. (H) Ratio of SSF1-GFP total fluorescence over cellular area as a function of generation

407 averaged after SEP alignment. N= 56 cells. (I) Ratio of nucleolar area (based on NET1-GFP
408 segmentation) over cellular area as a function of generation, averaged after SEP alignment.
409 N= 44 cells. (J) Mother cell with HTB2-sfGFP marker on a microfluidic chip before and after
410 SEP. (K) Ratio of nuclear area (based on HTB2-sfGFP segmentation) over cellular area (or N/C
411 ratio) as a function of generation, averaged after SEP alignment. N= 42 cells. (L) Model:
412 nucleolar stress precedes SEP during replicative aging. Scale bar: 5µm (for all pictures).

413 **Figure 4: rRNA synthesis and nuclear size are rejuvenated to basal levels in daughter cells of**
414 **aging mother.** (A) Left: Cell cycle duration of mother (green) and daughter (orange) cells as a
415 function of generation, averaged after SEP alignment. Right: normalized cell cycle duration of
416 daughters (orange) and mothers (green) for 4 classes of mother age. N= 29 cells. (B) Left:
417 picture of a senescent mother cell and its daughter cell with RPA190-GFP. Cell is delimited by
418 a yellow contour and fluorescence signal by a red contour. Middle: RPA190-GFP total
419 fluorescence in mothers (green) and daughters (orange) as a function of generation, averaged
420 after SEP alignment. Right: RPA190-GFP normalized fluorescence in mother (green) and
421 daughter (orange) cells for 4 classes of mother age. N= 21-61 cells. (C) Same as (B) for SSF1-
422 GFP marker. N= 17-56 cells. (D) Same as (B) for HTB2-sfGFP marker. N=42 cells. (E) Left: N/C
423 ratio of mother (green) and daughter (orange) cells as a function of generation, averaged after
424 SEP alignment. Right: N/C ratio of daughters (orange) and mothers (green) for 4 classes of
425 mother age. N= 42 cells. (F) Model: daughter cells of senescent mother do not inherit nucleolar
426 stress. Scale bar: 5µm (for all pictures).

427 **Figure 5: Senescence entry point results from a stochastic process dysregulating nucleolar**
428 **activity.** (A) Survival curves of fob1Δ strain (N= 126) and WT (N= 61). (B) and (C) Cell cycle
429 durations for 3 single cells of fob1Δ strain without any SEP before death (B) and with SEP (C).
430 (D) Cell cycle duration averaged after SEP alignment for WT (green, N= 57) and fob1Δ cells
431 with SEP (blue, N= 40). Fob1Δ cells without SEP (magenta, N= 84) were aligned from birth and
432 generation 0 was set to 30 (median SEP for fob1Δ cells with SEP). (E) and (F): Pictures of fob1Δ
433 cells with RPA190-GFP marker, just before death, without a SEP (E) and with a SEP (F). Cell is
434 delimited by a yellow contour and fluorescence signal by a red contour. Scale bar: 5µm. (G)
435 RPA190-GFP fluorescence and (H) HTB2-sfGFP fluorescence in WT (green), "fob1 with SEP"
436 (blue), "fob1 NO SEP" (magenta) after SEP alignment. N= 20-61 cells.

437 **Figure S1, related to Figure 1:** (A) From left to right: Total GFP-LacI fluorescence (arbitrary
438 units) within the contour delimited by NET1-mCherry signal for the same 3 single cells as in
439 Fig1, aligned from birth. Total GFP-LacI fluorescence averaged after birth alignment (N=49).
440 Total NET1-mCherry fluorescence for the same 3 single cells as in Fig1, aligned from birth.
441 Total NET1-mCherry fluorescence averaged after birth alignment (N=49). (B) Left: pictures of
442 a mother cell with FOB1-GFP marker in a microfluidic chip. Middle: total FOB1-GFP
443 fluorescence averaged after SEP alignment. Right: normalized FOB1-GFP fluorescence for 4
444 classes of age. N= 28 cells. Scale bar: 5µm. (C) Left: Cell area as a function of generation for 3
445 single cells (magenta, cyan, orange, same cells as in main Fig1) aligned from birth. Middle: Cell
446 area for the same 3 single cells aligned from SEP. Right: Cell area as a function of generation,
447 averaged after SEP alignment. (D) Left: segmented area of NET-mCherry signal for the same 3
448 single cells as above and main Fig1 aligned from SEP. Middle: averaged segmented area of

449 NET1-mCherry after SEP alignment. Right: normalized NET1-mCherry segmented area for 4
450 classes of age. N= 49. (E) Left: NET1-mCherry (top) and GFP-LacI (bottom) mean nucleolar
451 fluorescence for the same 3 single cells as a function of generation, after SEP alignment.
452 Middle: averaged mean fluorescence of NET1-mCherry (red) and GFP-LacI (green) as a
453 function of generation, after SEP alignment. Right: normalized mean fluorescence of NET1-
454 mCherry (red) and GFP-LacI (green) for 4 classes of age. N= 49 cells.

455 **Figure S2, related to Figure 3:** (A) Normalized ratio of NOG2-GFP total fluorescence over
456 cellular area for 4 classes of age. (B) Same as (A) for RPL13A-GFP. (C) Normalized growth rate
457 for 4 classes of age. (D) Same as (A) for RPA190-GFP. (E) Same as (A) for SSF1-GFP. (F) From
458 left to Right: pictures of a mother cell with ACT1pr-NLS-sfGFP, trapped in a cavity, before and
459 after SEP. NLS-sfGFP total fluorescence and N/C ratio (calculated from NLS-sfGFP
460 segmentation) as a function of generation, averaged after SEP alignment. Normalized N/C
461 ratio for 4 classes of mother age. N= 14 cells. (G) Same as (F) for ACT1pr-sfGFP marker instead
462 of ACT1pr-NLS-sfGFP. N= 28 cells. (H) From left to Right: pictures of a mother cell with VPH1-
463 GFP, trapped in a cavity, before and after SEP. VPH1-GFP total fluorescence and
464 vacuolar/cellular ratio as a function of generation after SEP alignment. Normalized
465 vacuolar/cellular ratio for 4 classes of mother age. N= 26 cells. Scale bar: 5µm (for all pictures).

466 **Figure S3, related to Figure 5:** (A) Cell area in fob1Δ (N= 64 cells) and WT (N= 123 cells) after
467 birth alignment. (B) Cell area in fob1Δ and WT after SEP alignment. (C) RPA190-GFP
468 fluorescence in daughter cells for WT (green, N= 21 cells), "fob1 with SEP" (blue, N= 12 cells),
469 "fob1 NO SEP" (magenta, N= 8 cells) after SEP alignment. (D) Growth rate (measured from
470 projected area) as a function of generation, averaged after SEP alignment for WT (green, N=
471 36 cells), "fob1 with SEP" (blue, N= 22 cells), "fob1 NO SEP" (magenta, N= 18 cells).

472 **Table1: aging parameters of the strains used in this study**

strain	N	RLS	% NO SEP	RLS NO SEP	RLS with SEP	SEP
BY4742	61	29	7	35	28	20
fob1Delta	126	36	68.3	37	34	30
NET1-GFP	51	19	9.8	14	19	14.5
fob1D+NET1-GFP	135	43	58	48	37	30
RPA190-GFP	78	19	11.5	13	19	14
fob1D+RPA190-GFP	101	34	64.4	39	22.5	21
HTB2-sfGFP	112	27.5	18.75	39	26	19
fob1D+HTB2-sfGFP	56	39	62.5	45	33	27

473

474 **Movie S1, related to Figure1**: Mother cell trapped in a cavity from birth to death and
475 containing the fluorescence markers GFP-LacI (with LacO on each rDNA repeat) and Net1-
476 mCherry. Time-lapse video. Left: phase contrast; middle: GFP; right: mCherry; cellular
477 contour is delimited in yellow. Scale bar: 5µm.

Movie S2, related to Figure2: Mother cell trapped in a cavity from birth to death and containing the fluorescence marker RPA190-GFP. Time-lapse video. Left: phase contrast; right: RPA190-GFP; cellular contour is delimited in yellow. Scale bar: 5µm.

Movie S3, related to Figure2: Mother cell trapped in a cavity from birth to death and containing the fluorescence marker SSF1-GFP. Time-lapse video. Left: phase contrast; right: SSF1-GFP; cellular contour is delimited in yellow. Scale bar: 5µm.

Movie S4, related to Figure3: Mother cell trapped in a cavity from birth to death and containing the fluorescence marker NOG2-GFP. Time-lapse video. Left: phase contrast; right: NOG2-GFP; cellular contour is delimited in yellow. Scale bar: 5µm.

Movie S5, related to Figure3: Mother cell trapped in a cavity from birth to death and containing the fluorescence marker RPL13A-GFP. Time-lapse video. Left: phase contrast; right: RPL13A-GFP; cellular contour is delimited in yellow. Scale bar: 5µm.

Movie S6, related to Figure3: Mother cell trapped in a cavity from birth to death and containing the fluorescence marker HTB2-sfGFP. Scale bar: 5µm.

Movie S7, related to Figure5: fob1Δ mother cell, containing the fluorescence marker RPA190-GFP, which does not enter into senescence before death. Scale bar: 5µm.

Movie S8, related to Figure5: fob1Δ mother cell, containing the fluorescence marker RPA190-GFP, which experiences SEP before death. Scale bar: 5µm.

Material and Methods

Yeast strains, plasmids and media

All strains used in this study are congenic to S288C, except TMY8-BY4B (strain TMY8 back-crossed 4 times with BY4742/41). All GFP-labeled strains were provided from M. Knop GFP collection. Fob1Δ strain was purchased from Euroscarf, crossed with strains containing relevant GFP markers and genotyped by PCR. The HTB2-sfGFP, Act1pr-sfGFP and Act1pr-NLS-GFP strains were generated using DNA editing and yeast genetics techniques.

Prior to loading into microfluidic chips, freshly thawed cells were grown overnight and then diluted in the morning to allow a few divisions in exponential growth.

RNA FISH buffers:
-Buffer B: 54.66g sorbitol + 25ml Phosphate Buffer + 195ml sterile water (250ml final volume)
-Phosphate buffer: 136.09g KH2PO4 +228.23g K2HPO4 (1L final volume)
-Zymolase mix: 2ml buffer B + 4µL PMSF (stock: 0.1M) + 20µL Vanadium (stock: 200mM) + 4µL βME (stock: 14.3M pur) + 20µL Zymolase 100T (stock 5mg/ml in water)
-20x SSC: 175.3g NaCl + 82.3g Sodium tri Citrate + adjust to 1L with H2O
-Hybridation mix solution A: 4µl FISH probe (stock 10ng/µl) + 8µl pur formamide + 4µl 2xSSC + 4µl tRNA (stock 10mg/ml) + 14µl H2O
-Hybridation mix solution B: 2µl BSA (5% in 4xSSC) + 4µl Vanadium (stock: 200mM) + 40µL 4xSSC.
To prepare hybridation mix, solution A was incubated 5min at 98°C then added to solution B at RT.

517
518 FISH probe sequence: GCACAGAAATCTCTCACCGTTTGGAATAGCAAGAAAGAAACTTACAAGC
519 with Cy3 dye in 5'. The probe targets ITS1 region between the A2 cleavage site and the 18S coding
520 region.
521
522 **Microfluidics**

523 The microfluidic master mold was made using standard soft-lithography techniques in the
524 FEMTO-ST nanotechnology platform of the French Renatech network (Besançon, France).
525 Prototypic molds were replicated in epoxy to ensure long-term preservation. The micro-
526 channels were cast by curing PDMS (Sylgard 184, 10:1 mixing ratio) and then covalently bound
527 to a 24 × 50 mm coverslip using plasma surface activation (Diener, Germany). The assembled
528 chip was then baked 1 hour at 60°C to consolidate covalent bonds between glass and PDMS
529 and then perfused with media circulating in Tygon tubing with a peristaltic pump (Ismatec,
530 Switzerland) at a 10µL/min flow rate. After 2 hours of PDMS rehydration, yeast cells were
531 loaded to the chip with a 1ml syringe and a 23G needle.

532 **Time-Lapse Microscopy**

533 All experiments have been replicated at least twice.

534 Cells were imaged using an inverted Nikon Ti-E microscope. Fluorescence illumination was
535 achieved using LED light (Lumencor) and light was collected using a 60× N.A. 1.4 objective and
536 a CMOS camera Hamamatsu Orca Flash 4.0. We used an automated stage in order to follow
537 up to 60 positions in parallel over the course of the experiment. Images were acquired every
538 10 or 15 min for a total duration of 140 hours (full lifespan) or 60 hours (RNA FISH) using NIS
539 software. Focus was maintained with the Nikon Perfect Focus System. A constant temperature
540 of 30°C was maintained on the chip using custom sample holder with thermoelectric modules,
541 an objective heater with heating resistors and a PID controller (5C7-195, Oven Industries).

542 **Image Analysis**

543 After acquisition, NIS raw data were analyzed using custom matlab software: phylocell and
544 autotrack available on //github.com/gcharvin. Cell contours and fluorescent markers were
545 segmented using a watershed algorithm and tracking was achieved with the Hungarian
546 method.

547 **RNA FISH on CHIP**

548 Time-lapse was stopped after 60 hours acquisition. 4% paraformaldehyde was perfused in the
549 chip for 30 min at RT for cell fixation then the chip was washed with buffer B for 20min. Cell
550 wall was digested by flowing zymolase mix for 20 min at RT followed by a 20min wash of buffer
551 B. We then rinsed the chip with cold 70% ethanol for 5min, then 15min with 2xSSC, then 20min
552 with 10% formamide in 2xSSC. Hybridation mix with 1ng/µl FISH probe was injected into the
553 chip which was then kept at 37°C for 3hours. After hybridation, we rinsed the chip 30 min with
554 warm (37°C) 10% formamide in 2xSSC, then 20 min with Triton X-100 (1% in 2xSSC) and finally
555 30min with 1xSSC. Cells in the chip were then imaged on a Nikon Ti-Eclipse with a mCherry
556 filter to acquire FISH probe signal (50% led power, 300ms exposure time, binning 2x2) with a

557 GFP filter for RPA190-GFP/NET1-GFP signal (20% led power, 100ms exposure time, binning
558 2x2) and in phase contrast.

559 **Acknowledgements**

560 This work was partly supported by the French RENATECH network. We thank Denis Fumagalli
561 and the MEDIAPREP facility of IGBMC for preparing media. We thank Prof. Takehiko Kobayashi
562 for providing the strain TMY8. We are grateful to Theo Aspert, Basile Jacquel and Sophie
563 Quintin for careful reading of the manuscript.

564 **Author contributions**

565 SM, OG and GC designed the project. SM and SJ carried out research and analyzed data. SM
566 and ILS developed the "FISH on chip" methodology. AM designed the yeast strains used in this
567 study. SM wrote the manuscript.

568 **References**

569 Brewer, B.J., and Fangman, W.L. (1988). A Replication Fork Barrier at the 3 'End of Yeast Ribosomal
570 RNA Genes. Cell *55*, 637-643.
571 Defossez, P.-A., Prusty, R., Kaeberlein, M., Lin, S.-J., Ferrigno, P., Silver, P.A., Keil, R.L., and Guarente,
572 L. (1999). Elimination of Replication Block Protein Fob1 Extends the Life Span of Yeast Mother Cells.
573 Molecular Cell *3*, 447-455.
574 Denoth-Lippuner, A., Krzyzanowski, M.K., Stober, C., and Barral, Y. (2014). Role of SAGA in the
575 asymmetric segregation of DNA circles during yeast ageing. Elife *3*.
576 Egilmez, N.K., and Jazwinski, S.M. (1989). Evidence for the Involvement of a Cytoplasmic Factor in the
577 Aging of the Yeast Saccharomyces cerevisiae. Journal of Bacteriology *171*, 37-42.
578 Fehrmann, S., Paoletti, C., Goulev, Y., Ungureanu, A., Aguilaniu, H., and Charvin, G. (2013). Aging
579 yeast cells undergo a sharp entry into senescence unrelated to the loss of mitochondrial membrane
580 potential. Cell Rep *5*, 1589-1599.
581 Gadal, O., Strauss, D., Petfalski, E., Gleizes, P.E., Gas, N., Tollervey, D., and Hurt, E. (2002). Rlp7p is
582 associated with 60S preribosomes, restricted to the granular component of the nucleolus, and
583 required for pre-rRNA processing. J Cell Biol *157*, 941-951.
584 Ganley, A.R., Ide, S., Saka, K., and Kobayashi, T. (2009). The effect of replication initiation on gene
585 amplification in the rDNA and its relationship to aging. Mol Cell *35*, 683-693.
586 Ganley, A.R., and Kobayashi, T. (2014). Ribosomal DNA and cellular senescence: new evidence
587 supporting the connection between rDNA and aging. FEMS Yeast Res *14*, 49-59.
588 Goulev, Y., Morlot, S., Matifas, A., Huang, B., Molin, M., Toledano, M.B., and Charvin, G. (2017).
589 Nonlinear feedback drives homeostatic plasticity in H2O2 stress response. Elife *6*.
590 Ide, S., Saka, K., and Kobayashi, T. (2013). Rtt109 prevents hyper-amplification of ribosomal RNA
591 genes through histone modification in budding yeast. PLoS Genet *9*, e1003410.
592 Janssens, G.E., Meinema, A.C., Gonzalez, J., Wolters, J.C., Schmidt, A., Guryev, V., Bischoff, R., Wit,
593 E.C., Veenhoff, L.M., and Heinemann, M. (2015). Protein biogenesis machinery is a driver of
594 replicative aging in yeast. Elife *4*, e08527.
595 Janssens, G.E., and Veenhoff, L.M. (2016). The Natural Variation in Lifespans of Single Yeast Cells Is
596 Related to Variation in Cell Size, Ribosomal Protein, and Division Time. PLoS One *11*, e0167394.
597 Jorgensen, P., Edgington, N.P., Schneider, B.L., Rupes, I., Tyers, M., and Futcher, B. (2007). The Size of
598 the Nucleus Increases as Yeast Cells Grow Mol Biol Cell *18*, 3523-3532.
599 Kennedy, B.K., Austriaco Jr., N.R., and Guarente, L. (1994). Daughter Cells of Saccharomyces
600 cerevisiae from Old Mothers Display a Reduced Life Span The Journal of Cell Biology *127*, 1985-1993.
601 Kobayashi, T. (2003). The Replication Fork Barrier Site Forms a Unique Structure with Fob1p and
602 Inhibits the Replication Fork. Molecular and Cellular Biology *23*, 9178-9188.

603 Kobayashi, T. (2008). A new role of the rDNA and nucleolus in the nucleus—rDNA instability
604 maintains genome integrity. BioEssays *30*, 267-272.
605 Kobayashi, T., Heck, D.J., Nomura, M., and Horiuchi, T. (1998). Expansion and contraction of
606 ribosomal DNA repeats in Saccharomyces cerevisiae: requirement of replication fork blocking (Fob1)
607 protein and the role of RNA polymerase I. Genes & Dev *12*, 3821-3830.
608 Kressler, D., Hurt, E., and Bassler, J. (2017). A Puzzle of Life: Crafting Ribosomal Subunits. Trends
609 Biochem Sci *42*, 640-654.
610 Kume, K., Cantwell, H., Neumann, F.R., Jones, A.W., Snijders, A.P., and Nurse, P. (2017). A systematic
611 genomic screen implicates nucleocytoplasmic transport and membrane growth in nuclear size
612 control. PLoS Genet *13*, e1006767.
613 Lu, K.L., Nelson, J.O., Watase, G.J., Warsinger-Pepe, N., and Yamashita, Y.M. (2018).
614 Transgenerational dynamics of rDNA copy number in Drosophila male germline stem cells. Elife *7*.
615 Miyazaki, T., and Kobayashi, T. (2011). Visualization of the dynamic behavior of ribosomal RNA gene
616 repeats in living yeast cells. Genes Cells *16*, 491-502.
617 Mortimer, R.K., and Johnston, J.R. (1959). Life Span of Individual Yeast Cells. Nature *183*, 1751-1752.
618 Nakaoka, H., and Wakamoto, Y. (2017). Aging, mortality, and the fast growth trade-off of
619 Schizosaccharomyces pombe. PLoS Biol *15*.
620 Neumann, F.R., and Nurse, P. (2007). Nuclear size control in fission yeast. J Cell Biol *179*, 593-600.
621 Nishimura, K., Kumazawa, T., Kuroda, T., Katagiri, N., Tsuchiya, M., Goto, N., Furumai, R., Murayama,
622 A., Yanagisawa, J., and Kimura, K. (2015). Perturbation of ribosome biogenesis drives cells into
623 senescence through 5S RNP-mediated p53 activation. Cell Rep *10*, 1310-1323.
624 Saka, K., Ide, S., Ganley, A.R., and Kobayashi, T. (2013). Cellular senescence in yeast is regulated by
625 rDNA noncoding transcription. Curr Biol *23*, 1794-1798.
626 Shcheprova, Z., Baldi, S., Frei, S.B., Gonnet, G., and Barral, Y. (2008). A mechanism for asymmetric
627 segregation of age during yeast budding. Nature *454*, 728-734.
628 Sinclair, D.A., and Guarente, L. (1997). Extrachromosomal rDNA Circles— A Cause of Aging in Yeast.
629 Cell *91*, 1033-1042.
630 Spivey, E.C., Jones, S.K., Rybarski, J.R., Saifuddin, F.A., and Finkelstein, I.J. (2017). An aging-
631 independent replicative lifespan in a symmetrically dividing eukaryote. Elife *6*.
632 Takeuchi, Y., Horiuchi, T., and Kobayashi, T. (2003). Transcription-dependent recombination and the
633 role of fork collision in yeast rDNA. Genes Dev *17*, 1497-1506.
634 Tiku, V., Jain, C., Raz, Y., Nakamura, S., Heestand, B., Liu, W., Spath, M., Suchiman, H.E.D., Muller,
635 R.U., Slagboom, P.E.*, et al.* (2016). Small nucleoli are a cellular hallmark of longevity. Nat Commun *8*,
636 16083.

637

Figure 1

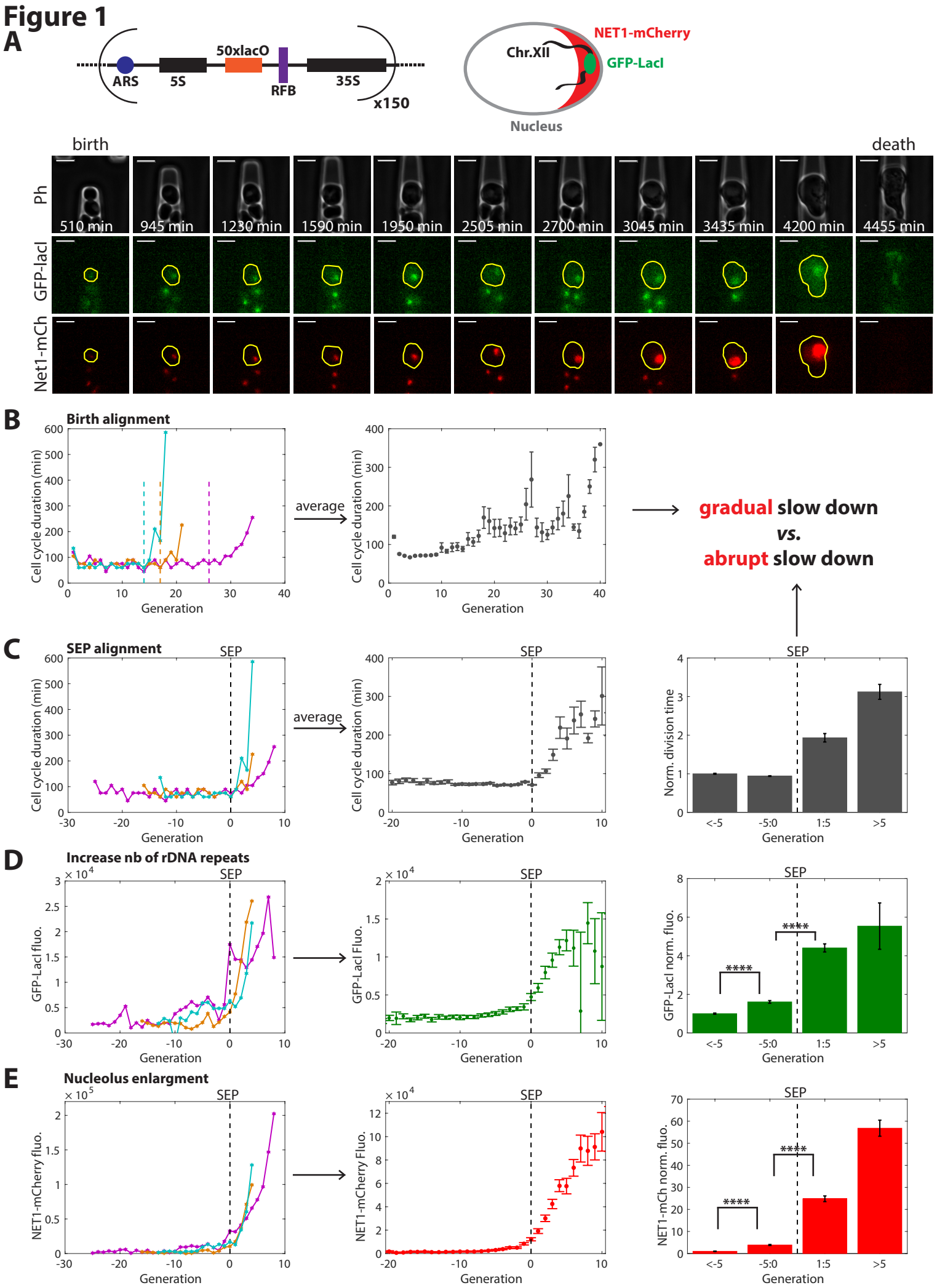
A
ARS
5S
50xlacO
RFB
35S
x150
Chr.XII
NET1-mCherry
GFP-LacI
Nucleus
birth
death
Ph
GFP-lacI
Net1-mCh
510 min
945 min
1230 min
1590 min
1950 min
2505 min
2700 min
3045 min
3435 min
4200 min
4455 min
B
Birth alignment
Cell cycle duration (min)
Generation
average
gradual slow down
vs.
abrupt slow down
C
SEP alignment
SEP
Norm. division time
<-5
-5:0
1:5
>5
D
Increase nb of rDNA repeats
GFP-LacI fluo.
GFP-LacI Fluo.
GFP-LacI norm. fluo.
****
E
Nucleolus enlargment
NET1-mCherry fluo.
NET1-mCherry Fluo.
NET1-mCh norm. fluo.

Figure 2

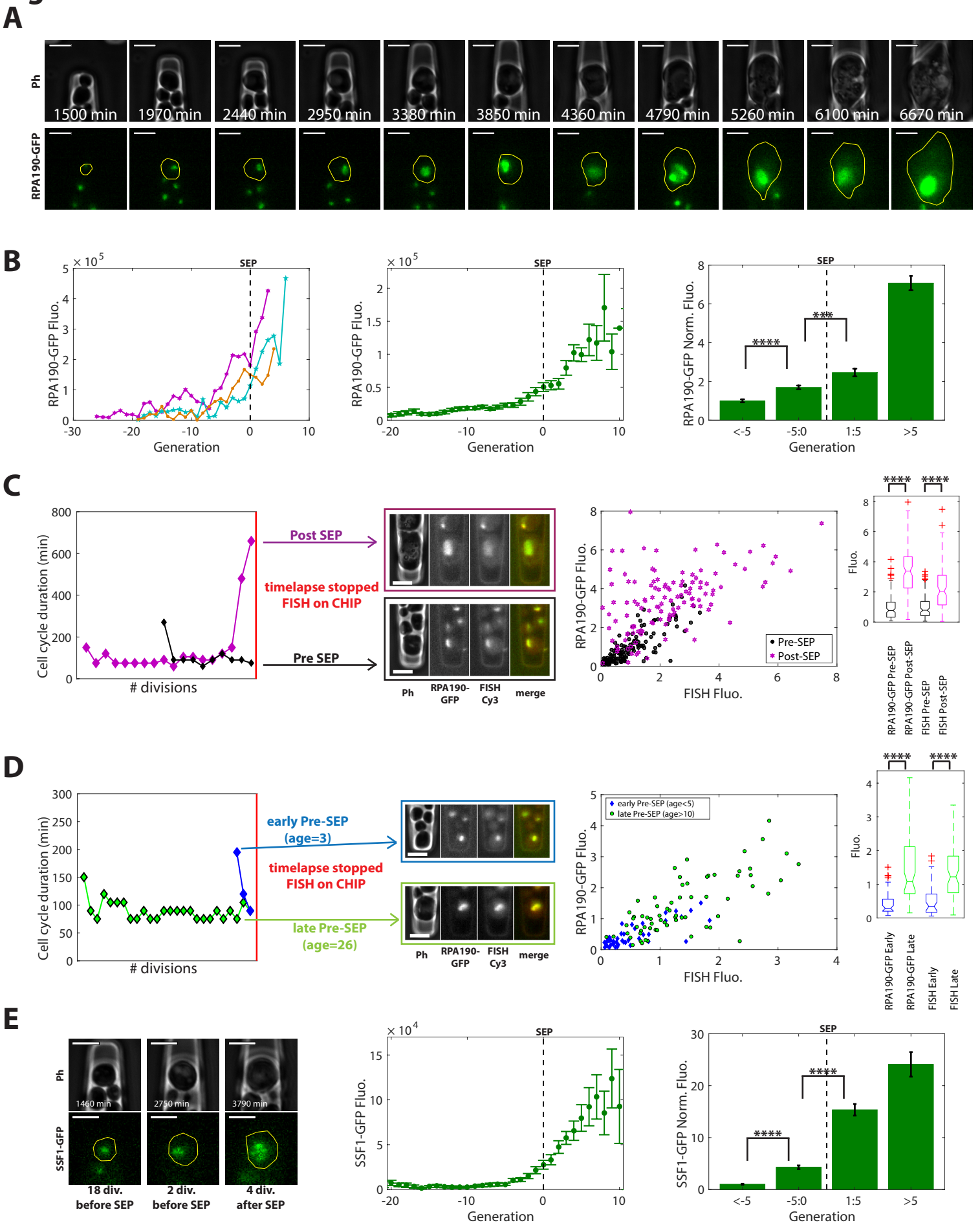
A
Ph
RPA190-GFP
1500 min
1970 min
2440 min
2950 min
3380 min
3850 min
4360 min
4790 min
5260 min
6100 min
6670 min
B
RPA190-GFP Fluo.
Generation
SEP
RPA190-GFP Norm. Fluo.
<-5
-5:0
1:5
>5
C
Cell cycle duration (min)
divisions
Post SEP
timelapse stopped
FISH on CHIP
Pre SEP
Ph
RPA190-GFP
FISH Cy3
merge
FISH Fluo.
Pre-SEP
Post-SEP
Fluo.
RPA190-GFP Pre-SEP
RPA190-GFP Post-SEP
FISH Pre-SEP
FISH Post-SEP
D
early Pre-SEP
(age=3)
late Pre-SEP
(age=26)
early Pre-SEP (age<5)
late Pre-SEP (age>10)
RPA190-GFP Early
RPA190-GFP Late
FISH Early
FISH Late
E
SSF1-GFP
18 div.
before SEP
2 div.
before SEP
4 div.
after SEP
SSF1-GFP Fluo.
SSF1-GFP Norm. Fluo.

Figure 3

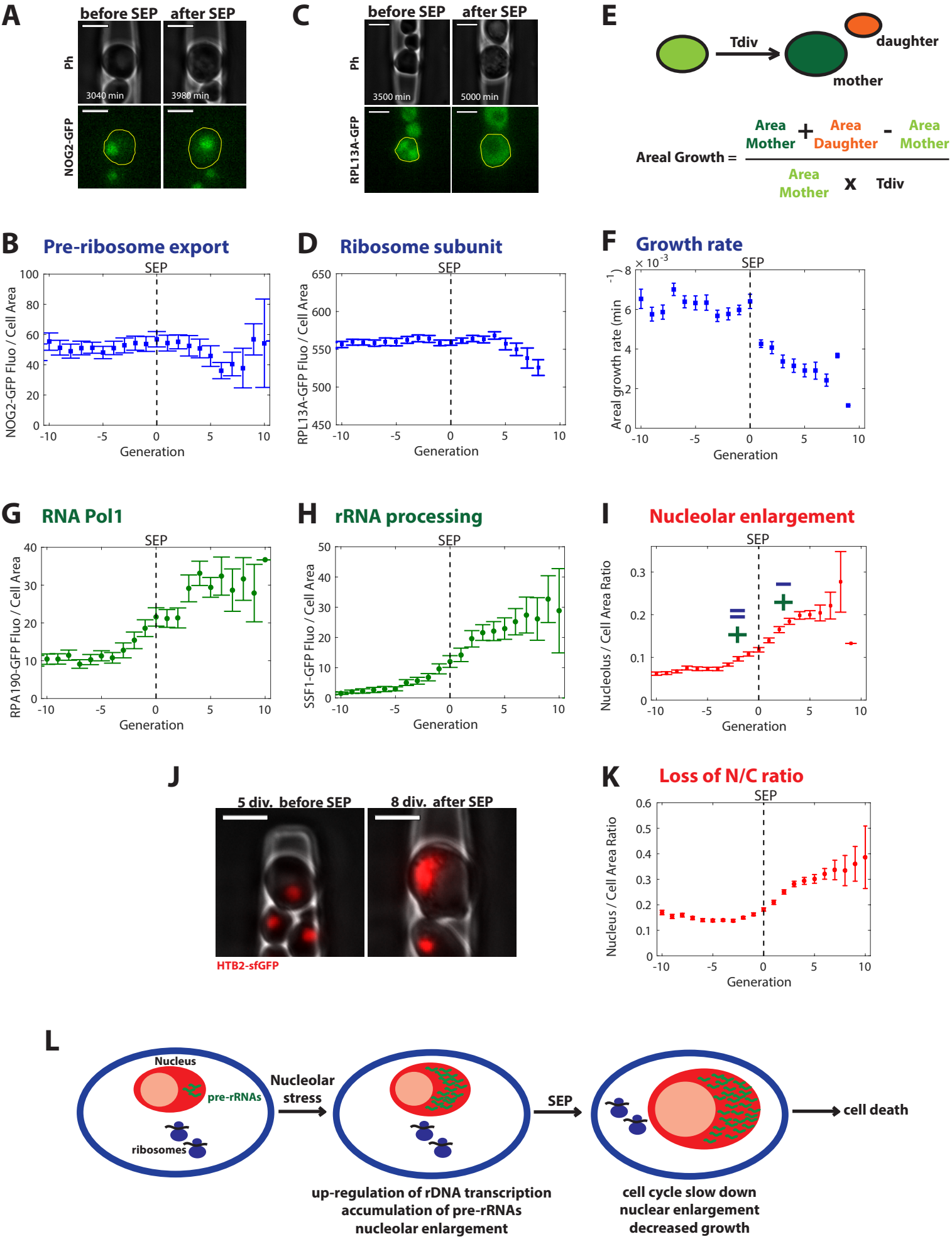
A
before SEP
after SEP
Ph
NOG2-GFP
3040 min
3980 min
C
before SEP
after SEP
Ph
RPL13A-GFP
3500 min
5000 min
E
Tdiv
daughter
mother
Areal Growth = (Area Mother + Area Daughter - Area Mother) / (Area Mother x Tdiv)
B
Pre-ribosome export
SEP
NOG2-GFP Fluo / Cell Area
Generation
D
Ribosome subunit
SEP
RPL13A-GFP Fluo / Cell Area
Generation
F
Growth rate
SEP
Areal growth rate (min -1)
Generation
G
RNA Pol1
SEP
RPA190-GFP Fluo / Cell Area
Generation
H
rRNA processing
SEP
SSF1-GFP Fluo / Cell Area
Generation
I
Nucleolar enlargement
SEP
Nucleolus / Cell Area Ratio
Generation
J
5 div. before SEP
8 div. after SEP
HTB2-sfGFP
K
Loss of N/C ratio
SEP
Nucleus / Cell Area Ratio
Generation
L
Nucleus
pre-rRNAs
ribosomes
Nucleolar stress
SEP
cell death
up-regulation of rDNA transcription
accumulation of pre-rRNAs
nucleolar enlargement
cell cycle slow down
nuclear enlargement
decreased growth

Figure 4

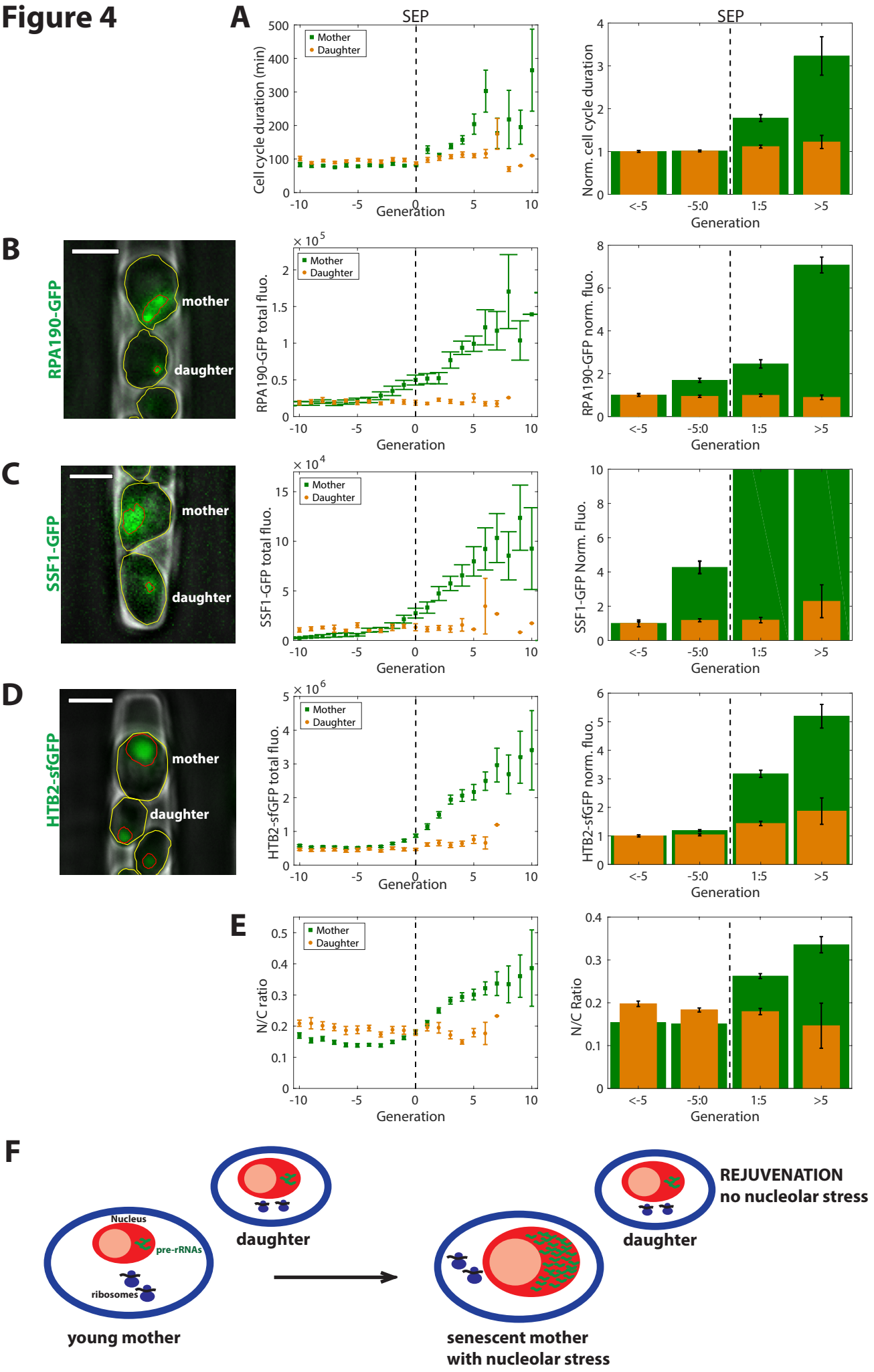
A
SEP
Mother
Daughter
Cell cycle duration (min)
Generation
Norm. cell cycle duration
<-5
-5:0
1:5
>5
B
RPA190-GFP
mother
daughter
RPA190-GFP total fluo.
RPA190-GFP norm. fluo.
C
SSF1-GFP
SSF1-GFP total fluo.
SSF1-GFP Norm. Fluo.
D
HTB2-sfGFP
HTB2-sfGFP total fluo.
HTB2-sfGFP norm. fluo.
E
N/C ratio
N/C Ratio
F
Nucleus
pre-rRNAs
ribosomes
young mother
daughter
senescent mother
with nucleolar stress
REJUVENATION
no nucleolar stress

Figure 5

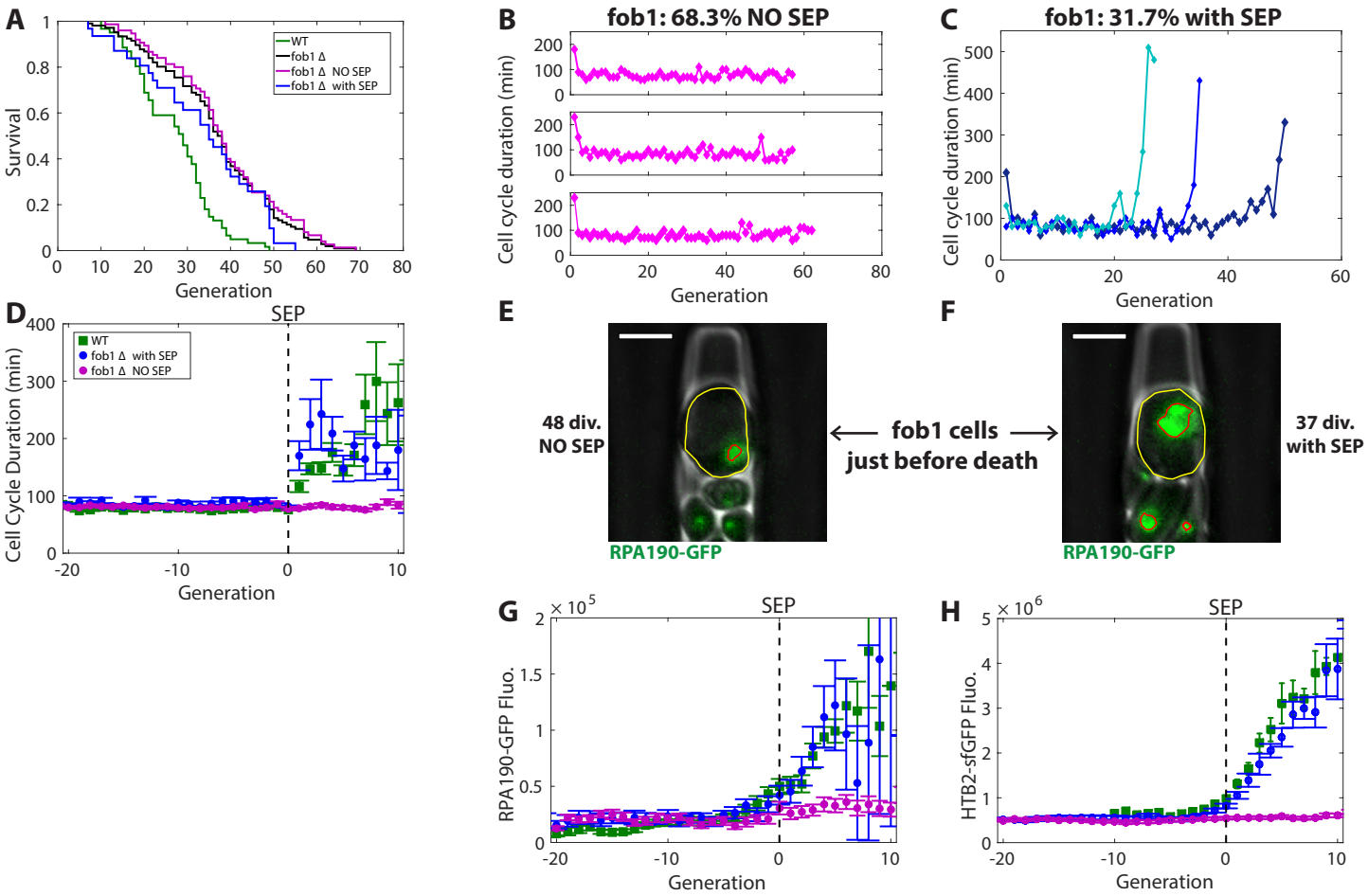
A
Survival
Generation
WT
fob1 Δ
fob1 Δ NO SEP
fob1 Δ with SEP
B
fob1: 68.3% NO SEP
Cell cycle duration (min)
Generation
C
fob1: 31.7% with SEP
Cell cycle duration (min)
Generation
D
SEP
Cell Cycle Duration (min)
Generation
WT
fob1 Δ with SEP
fob1 Δ NO SEP
E
48 div.
NO SEP
RPA190-GFP
fob1 cells
just before death
F
37 div.
with SEP
RPA190-GFP
G
× 10^5
SEP
RPA190-GFP Fluo.
Generation
H
× 10^6
SEP
HTB2-sfGFP Fluo.
Generation

Figure S1

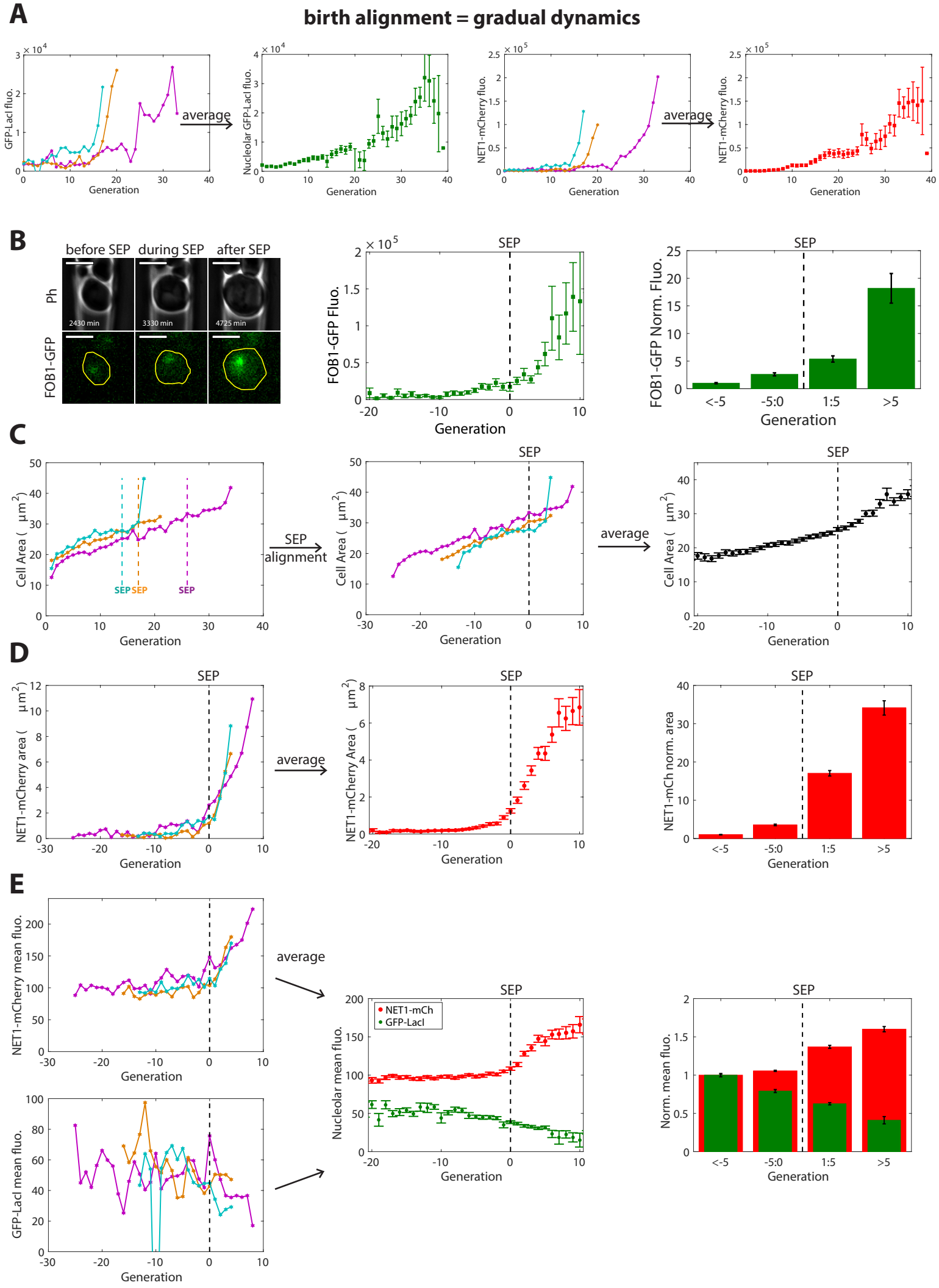
A
birth alignment = gradual dynamics
GFP-LacI fluo.
Generation
average
Nucleolar GFP-LacI fluo.
NET1-mCherry fluo.
B
before SEP
during SEP
after SEP
Ph
FOB1-GFP
2430 min
3330 min
4725 min
FOB1-GFP Fluo.
SEP
FOB1-GFP Norm. Fluo.
<-5
-5:0
1:5
>5
C
Cell Area (µm²)
SEP alignment
D
NET1-mCherry area (µm²)
NET1-mCherry Area (µm²)
NET1-mCh norm. area
E
NET1-mCherry mean fluo.
GFP-LacI mean fluo.
Nucleolar mean fluo.
NET1-mCh
GFP-LacI
Norm. mean fluo.

Figure S2

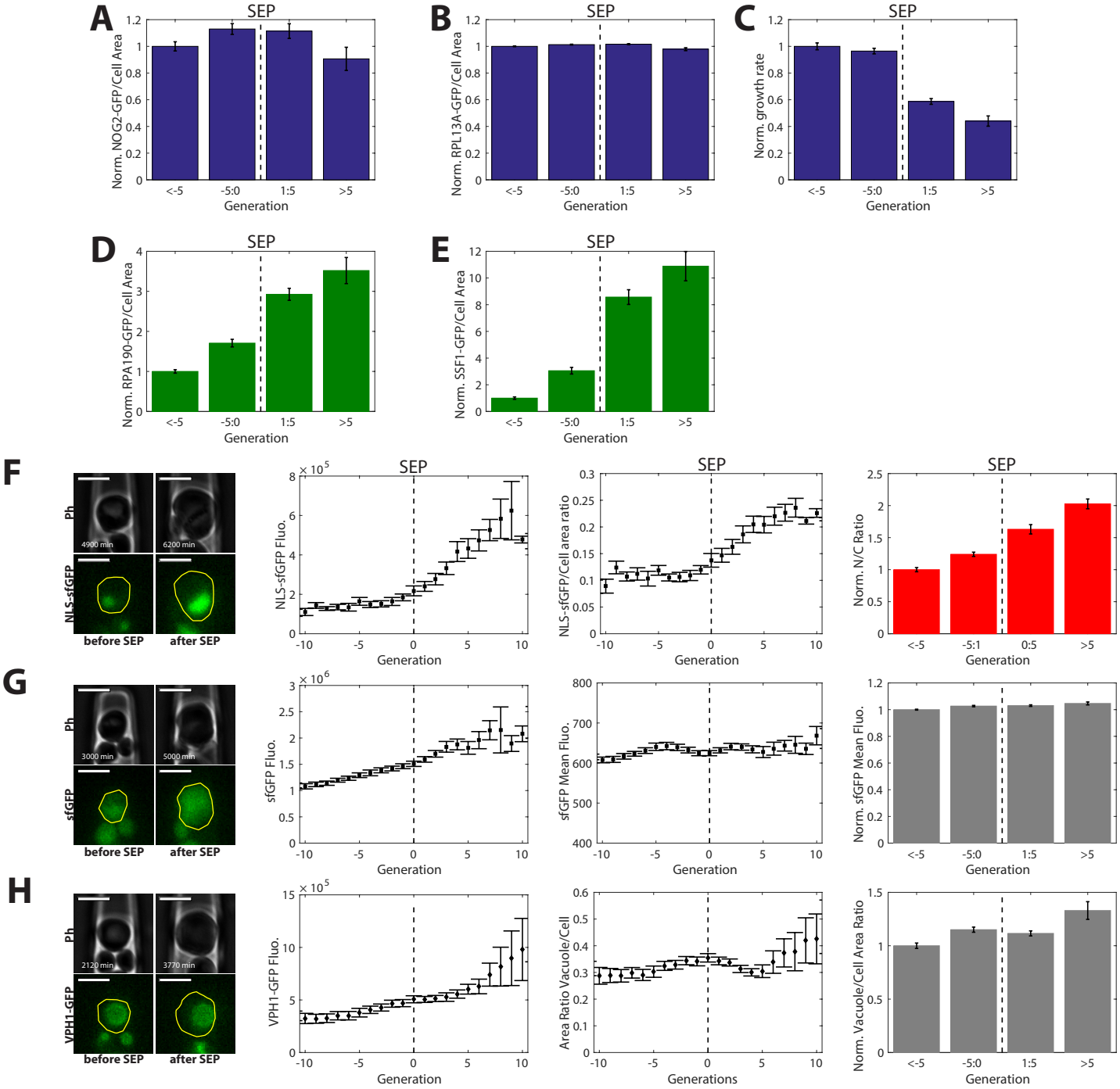
A
SEP
Norm. NOG2-GFP/Cell Area
<-5
-5:0
1:5
>5
Generation
B
SEP
Norm. RPL13A-GFP/Cell Area
C
SEP
Norm. growth rate
D
SEP
Norm. RPA190-GFP/Cell Area
E
SEP
Norm. SSF1-GFP/Cell Area
F
Ph
NLS-sfGFP
4900 min
6200 min
before SEP
after SEP
NLS-sfGFP Fluo.
NLS-sfGFP/Cell area ratio
Norm. N/C Ratio
-5:1
0:5
G
3000 min
5000 min
sfGFP
sfGFP Fluo.
sfGFP Mean Fluo.
Norm. sfGFP Mean Fluo.
H
2120 min
3770 min
VPH1-GFP
VPH1-GFP Fluo.
Area Ratio Vacuole/Cell
Generations
Norm. Vacuole/Cell Area Ratio

Figure S3

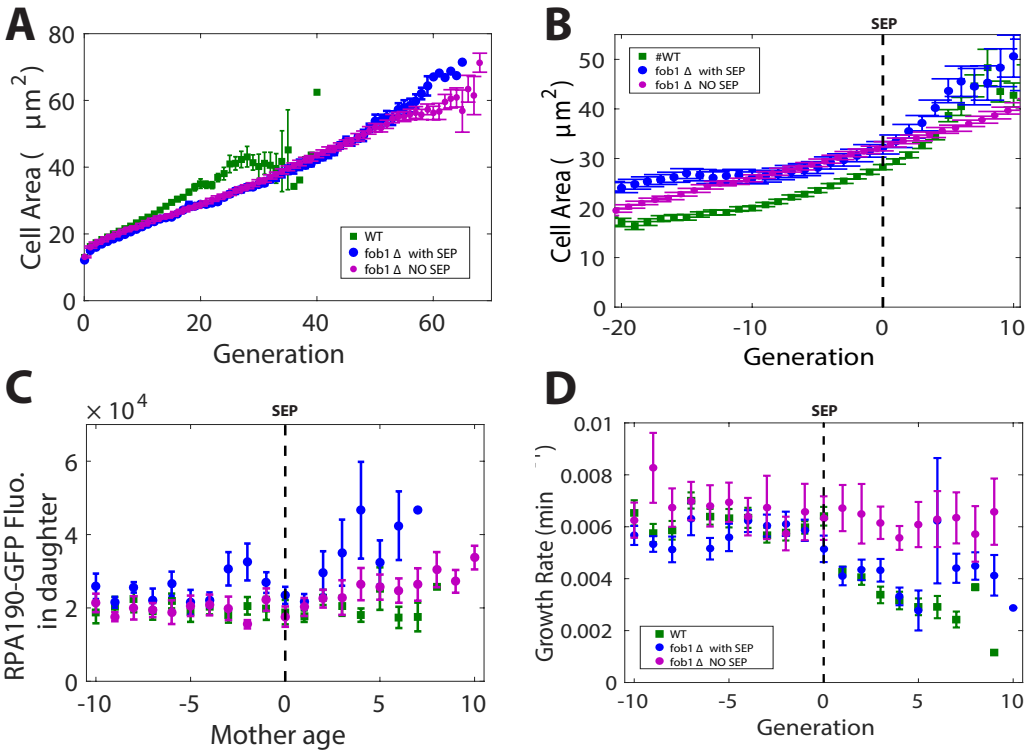
A
Cell Area (μm2)
Generation
WT
fob1 Δ with SEP
fob1 Δ NO SEP
B
SEP
#WT
fob1 Δ with SEP
fob1 Δ NO SEP
Cell Area (μm2)
Generation
C
× 10^4
SEP
RPA190-GFP Fluo. in daughter
Mother age
D
SEP
Growth Rate (min-1)
Generation
WT
fob1 Δ with SEP
fob1 Δ NO SEP